Knock-in rat lines with Cre recombinase at the dopamine D1 and adenosine 2a receptor loci.

Jeffrey R. Pettibone[1], Jai Y. Yu[2], Rifka C. Derman[6], Elizabeth D. Hughes[7], Wanda E. Filipiak[7], Michael G. Zeidler[7], Thomas L. Saunders[7,8], Carrie R. Ferrario[9] and Joshua D. Berke[1,3,4,5*]

[1]Department of Neurology, [2]Department of Physiology, [3]Department of Psychiatry, [4]Kavli Institute for Fundamental Neuroscience, [5]Weill Institute for Neurosciences, University of California, San Francisco, CA.

[6]Neuroscience Graduate Program, [7]Transgenic Animal Model Core, [8]Department of Internal Medicine, [9]Department of Pharmacology, University of Michigan, Ann Arbor, MI

*Corresponding author

ABSTRACT

Genetically-modified mice have been widely used in neuroscience. Our understanding of the basal ganglia in particular has been greatly assisted by BAC mutants with selective transgene expression in striatal neurons forming the direct or indirect pathways. However, for more sophisticated behavioral tasks and larger intracranial implants, rats are preferred. Furthermore, BAC lines can show variable expression patterns depending upon genomic insertion site. We therefore used CRISPR-Cas9 gene editing to generate two novel knock-in rat lines, specifically encoding *iCre* recombinase immediately after the dopamine D1 receptor *(Drd1a)* or adenosine 2a receptor (*Adora2a)* loci. We confirmed these rats show selective, functional Cre expression in the direct and indirect pathways respectively, using a combination of *in situ* hybridization and viral transfections. Finally, we verified normal movement, learning, and motivation across a range of behavioral paradigms. We expect these new D1-Cre and A2a-Cre rat lines to be widely used to study both normal brain functions and neurological and psychiatric pathophysiology.

INTRODUCTION

Dopamine and adenosine are important chemical messengers in the brain, vasculature, and elsewhere in the body. Within the brain, one key site of action is the striatum, a critical component of basal ganglia circuitry involved in movement, motivation, and reinforcement-driven learning(Berke, 2018). The majority (90-95%) of striatal neurons are medium spiny projection neurons (MSNs) that can be categorized into two distinct classes(Gerfen & Surmeier, 2011). “Direct pathway” neurons (dMSNs) express dopamine D1 receptors and project primarily to the substantia nigra pars reticulata / globus pallidus pars interna (SNr/GPi). “Indirect pathway” neurons (iMSNs) express both dopamine D2 receptors and adenosine A2a receptors, and project primarily to the globus pallidus pars externa (GPe). Although our understanding of their distinct functions is far from complete, dMSNs and iMSNs appear to have complementary roles promoting and discouraging motivated behaviors respectively(Collins & Frank, 2014).

Over the last decade the investigation of dMSNs and iMSNs has been transformed by transgenic animals. Mutant mice with random genomic insertion of BACs (bacterial artificial chromosomes) encoding dopamine receptor promoter sequences driving fluorescent protein expression confirmed the near-total segregation of striatal D1 and D2 receptors (Matamales et al., 2009; Shuen, Chen, Gloss, & Calakos, 2008). These mice have also been widely used for identification of dMSNs versus iMSNs in brain slice experiments (Day et al., 2006). BAC lines in which dopamine receptor promoters drive Cre recombinase expression (D1-Cre, D2-Cre, etc) have allowed *in vivo* identification, monitoring and manipulation of select neuronal subpopulations both in striatum (Barbera et al., 2016; Cui et al., 2013; Kravitz et al., 2010; Kravitz, Tye, & Kreitzer, 2012) and cortex (Y.-C. Kim et al., 2017). Note that for targeting iMSNs A2a-Cre mice are usually preferred over D2-Cre, since A2a receptors are selectively expressed on iMSNs while D2 receptors are also expressed on other striatal elements

including cholinergic interneurons (Alcantara, Chen, Herring, Mendenhall, & Berlanga, 2003).

However, for many types of experiment rats are more suitable than mice. Their larger size means they can bear more complex intracranial implants, including high-channel-count electrophysiology devices, without hindering mobility. Furthermore, rats can be more effectively trained in sophisticated behavioral tasks, including those investigating reinforcement learning (Hamid et al., 2016) and behavioral inhibition (Schmidt, Leventhal, Mallet, Chen, & Berke, 2013). The advent of CRISPR/Cas9 methods has greatly facilitated the generation of knock-in rat lines (Jung et al., 2016; Mali, Esvelt, & Church, 2013). The knock-in approach is also more likely to produce faithful expression patterns compared to BACs, for which (for example) different D1-cre lines show markedly different expression (Heintz, 2004).

Here we describe novel transgenic D1-Cre and A2a-Cre rat lines created using CRISPR/Cas9. After describing how they were made, we demonstrate selectivity and specificity of *iCre* mRNA expression to the intended striatal targets, Next, we use virus for Cre-dependent expression to confirm that Cre is both functional and appropriately confined to direct or indirect pathways. Finally, we use a set of behavioral tasks to demonstrate normal locomotor activity, learning and motivation. These new rats are likely to find wide application across many subfields of behavioral and systems neuroscience.

RESULTS

Molecular Design

The new rat lines were designed so that the native *Drd1a* (or *Adora2a)* promoter drives expression of both the native receptor and the codon-improved *Cre* recombinase *(iCre)* sequence in a single transcription event (Figure 1A). For each line, a unique single strand guide RNA was generated to induce double strand breaks at the terminus of the receptor coding sequence, and microinjected into Long Evans rat zygotes along with Cas9 and a circular plasmid containing the gene cassette. After insertion, the 3' end of

target receptor gene was followed by the "self-cleaving" peptide P2A (to separate the Cre protein after translation), followed by *iCre* recombinase with a nuclear localizing signal affixed at the amino terminus, and a peptide tag (HA for Adora2a, V5 for D1) to facilitate antibody-based detection.

Founder screening and germline transmission

DNA samples from G0 potential founders were screened with primers to detect the presence of *iCre* in the genome (for full primer sequences, see Methods). From this screen 21/96 potential D1-Cre, and 9/60 potential A2a-Cre founders were positive for *iCre*. Positive rats were then screened with additional primers across the junctions between native and introduced DNA stretches, to discriminate between correct and random genomic integration events. This yielded 7/21 correct D1-Cre insertions and 7/9 correct A2a-Cre insertions, and in these animals the *iCre* insert was completely sequenced to confirm complete integration of all necessary coding sequences.

These G0 founders were mated with Long Evans rats, and the G1 pups subjected to the *iCre* specific insertion genotyping process to verify germline transmission. Colonies from one successful founder for each line were established and maintained by always back-crossing to wild-type Long-Evans rats from commercial vendors; all experimental results shown are from rats after at least 3 generations of such back-crossing.

Consistent and specific Cre expression in *Drda1+ or Adora2a+* cells

Our design ought to produce *Drd1a* (or *Adora2a*) mRNA in 1:1 stoichiometry with *iCre* mRNA, and thus yield highly selective *iCre* expression. To assess this we used fluorescent *in situ* hybridization, together with DAPI labeling of cell nuclei. Probe sets targeting *iCre*, *Adora2a* receptor and *Drd1a* receptor mRNA with distinct color labels were all multiplexed and visualized simultaneously (Figure 2A). Images were analyzed for three distinct striatal subregions- the dorsal striatum (DS), the nucleus accumbens core, and the nucleus accumbens medial shell. Automated software was used to define cell boundaries and count fluorescent puncta per cell, for each probe (Figure 2B).

As expected, in D1-Cre rats expression of *Drd1a* and *iCre* mRNA was closely correlated in all striatal subregions examined (Fig. 2C; DS: R^2=0.79; Core: R^2=0.72; Shell: R^2=0.65), and there was no correlation between *Adora2a* and *iCre* mRNA (DS: R^2=0.0068; Core: R^2=0.021; Shell: R^2=0.014). Conversely in A2a-Cre rats expression of *Adora2a* and *iCre* mRNA was closely correlated (DS: R^2=0.94; Core: R^2=0.87; Shell: R^2=0.95), and there was no correlation between *Drd1a* and *iCre* mRNA (DS: R^2=0.03; Core: R^2=0.017; Shell: R^2=0.036). Consistent with earlier *in situ* hybridization studies (Berke, Paletzki, Aronson, Hyman, & Gerfen, 1998; Le Moine & Bloch, 1995) we found near-complete segregation of dMSN and iMSN markers in all regions examined, with virtually no overlap between *Drd1a* and *Adora2a* expression (Fig. 2A,C).

To further assess the specificity and consistency of *iCre* mRNA expression we defined thresholds for considering neurons as "positive" for a given probe. Given the wide distributions of puncta counts, the choice of threshold is non-trivial; it forces a tradeoff between type I and type II errors. For quantification we applied a uniform threshold for all mRNAs, the 99.9% upper confidence limit for each probe, assuming a Poisson distribution of puncta per cell. Using these thresholds we estimated A2a-Cre specificity (% of *iCre*+ that are also *Adora2a*+) to be 94.4% (DS), 92.0% (core), and 94.6% (shell), and consistency (% of *Adora2a*+ that are also *iCre*+) as 94.6% (DS), 83.9% (core), and 89.0% (shell). In the D1-Cre line, we estimated specificity to be 97.8% (DS), 94.6% (core) and 97.1% (shell), and consistency to be 62.5% (DS), 55.6% (core) and 51.2% (shell). These lower consistency numbers for D1-Cre may partly reflect noisier *Drd1a* labeling. With even higher thresholds for *Drd1a* (e.g. >35 puncta / cell) we can be essentially certain of cell identity, and assessed this way consistency and specificity were both close to 100% (Fig. 2c).

We next examined whether this *iCre* expression results in functional Cre protein that is confined to the appropriate basal ganglia pathway. We injected adeno-associated virus carrying CAG-Flex-TdTomato into dSTR, and examined the pattern of expression after 4 weeks of transfection. As expected, injections into the D1-Cre line resulted in clear Cre-dependent TdTomato labeling of the striatonigral axon pathway (Figure 2C). Virus injections into dSTR in the A2a-Cre line produced labeling in both dSTR and GPe,

but none in the SNr, consistent with selective expression in the striatopallidal pathway. These results confirm functional Cre protein in each line with appropriate pathway-specific expression.

Transgenic lines show normal learning, motivation, and cocaine-induced locomotor activity.

As these transgenic lines are likely to find wide application in studies of movement, motivation, learning and dopamine function, we performed some basic tests to gain confidence that they behave normally.

To quantify any changes in baseline movement, or movement under dopaminergic challenge, we placed Cre+ rats and their Cre- littermates in an operant chamber and examined locomotor behavior in the context of saline and cocaine. In the first session, rats were habituated to the chamber and the injection procedure by receiving IP saline 30 and 75 minutes after the start of the session. As expected, locomotor activity decreased across time after each injection and did not differ between genotypes, indicating that our lines show normal baseline locomotion (Figure 3A, Two-way repeated-measures ANOVA, main effect of time: $F_{(21,378)} = 10.42$, $p<0.0001$; n.s. effect of genotype: $F_{(2, 18)} = 0.3965$, $p=0.6784$).

In a second session, rats were again given an acute IP injection of saline 30 minutes into the session but received IP cocaine in a second injection 45 minutes later. Locomotor activity changed across time, but did not differ between genotypes across testing (Figure 3B, Two-way repeated-measures ANOVA, main effect of time: $F_{(23,414)} = 6.901$, $p<0.0001$; n.s. effect of genotype: $F_{(2, 18)} = 0.09284$, $p=0.9118$). To assess the effect of saline vs cocaine injections, we compared locomotion in the 45 minutes following each injection. All genotypes showed a significant increase in locomotor activity following cocaine vs saline injections and this effect did not differ between genotypes, demonstrating a similar sensitivity to the elevated dopamine irrespective of genotype (Figure 3C, Two-way repeated-measures ANOVA, main effect of injection:

$F_{(1,18)}$ = 10.51, p=0.0045; n.s. effect of genotype: $F_{(2, 18)}$ = 0.1284, p=0.8803; n.s. injection by genotype interaction: $F_{(2, 18)}$ = 0.1122, p=0.8945).

We next used an instrumental discrimination task to determine whether our lines show motivational or learning deficits in reinforcement-driven responding. In an operant chamber presses on an active lever were reinforced with pellets, but presses on an inactive lever were never reinforced. Rats were required to reach an acquisition criterion of earning 50 pellets consecutively within less than 40 minutes. Active lever responding was greater than inactive lever responding and this did not differ between genotypes (Figure 4A, Two-way repeated-measures ANOVA main effect of lever: $F_{(1, 90)}$ = 193.2, p<0.0001; n.s. main effect of genotype: $F_{(3, 90)}$ = 1.379, p=0.2545; n.s. genotype x lever interaction: $F_{(3, 90)}$ = 0.408, p=0.747). The time to reach the acquisition criterion also did not differ between genotypes, indicating similar learning and motivation (Figure 4B, One-way ANOVA; $F_{(3, 45)}$= 1.611, p=0.200).

To assess Pavlovian approach learning, the same rats were conditioned to discriminate between one auditory cue that was paired with food pellet delivery (conditioned stimulus: CS+), and a second auditory cue that was never paired with food (CS-). Each CS was presented for 2 minutes and pellet delivery occurred 15-45 s after CS+ onset. Anticipatory conditioned responding was assessed during the first 10 s. Acquisition of Pavlovian conditioned food cup approach was similar across strains and between *Cre*- vs. *Cre*+ groups. Figure 4C and 4D shows the average number of food cup entries during the first 10 s of CS+ and CS- in 2-session blocks, respectively. Anticipatory food cup responding to CS+ presentations increased across training blocks and did not differ between groups, indicating that all groups learned the value of the CS+ at equal rates and were similarly motivated to respond (Figure 4C: Two-way RM ANOVA: main effect of training block $F_{(5,225)}$ = 13.45 p<0.0001; n.s. main effect of group $F_{(3,45)}$ = 0.505, p=0.6807; n.s. group x training block interaction $F_{(15,225)}$ =0.6086, p=0.866). Food cup responding during the first 10 seconds of CS- presentations did not increase across sessions and did not differ between groups (Figure 4D: Two-way RM ANOVA n.s. main effect of training block $F_{(5,225)}$ = 1.602 p=0.1606; n.s. main effect of group $F_{(3,45)}$ = 0.01628, p=0.9971; n.s. group x training block interaction $F_{(15,225)}$ =1.476, p=0.1155).

To provide an additional measure of learning we also recorded the latency to enter the food cup following CS presentations. The average latency to enter the food cup following the onset of the CS+ decreased across training blocks and this decrease did not differ between groups, again demonstrating that all groups were similarly motivated to respond to reward predictive cues (Figure 4F: Two-way RM ANOVA main effect of training block $F_{(5,225)} = 16.95$, $p<0.0001$; n.s. main effect of group $F_{(3,45)} = 1.239$, $p=0.307$; n.s. group x training block interaction $F_{(15, 225)} =0.3964$, $p=0.9791$). In contrast, the average latency to enter the food cup following the onset of the CS- increased across training blocks, and did not differ between groups (Figure 4G Two-way RM ANOVA main effect of training block $F_{(5,225)} = 12.38$, $p<0.0001$; n.s. main effect of group $F_{(3,45)} = 0.6639$, $p=0.578$; n.s. group x training block interaction $F_{(15,225)} =0.4812$, $p=0.9485$). Together, the results of these behavioral tasks indicate that our new lines show appropriate movement, motivation, learning, and responses to dopaminergic intervention.

DISCUSSION

We have demonstrated successful, functional knock-in of Cre recombinase in two novel rat lines. Normal behavioral performance in a range of assays provides further confidence that there are no other unintended deleterious effects of genetic manipulation. Within striatum we showed that expression of Cre was consistent and selective to the correct populations of projection neurons. Thus, these D1-Cre and A2a-Cre rats enable selective manipulation of dMSNs and iMSNs with high specificity, and offer some clear advantages over currently available models.

First, the capacity for rats to learn complex unrestrained behaviors make them stronger candidates for a wider range of tasks compared to mice. Second, the increased carrying capacity afforded by rats facilitates the chronic implantation of larger devices (i.e. high channel-count headstages, graded-index (GRIN) lenses). Thirdly, knock-ins can be used with higher confidence that the genetic modification was selective and specific to the target, compared to BAC lines.

Despite using CRISPR/Cas9 technology, there remains the chance for off-target effects from the editing process due to limitations of the sgRNA ability to be mated exclusively to the insertion site. To minimize any unintended near-insertion effects, we ran multiple near-insertion PCRs at both junctions of the insertion during the G0 screening. To minimize unintended effects further from the insertion, we have back-crossed each successive generation to a wild-type Long Evans rat.

A common concern when studying MSNs is the degree of overlapping D1 and D2 receptor expression. Overlap in BAC transgenic mice has been reported to range from 5-17% across striatal subregions (Bertran-Gonzalez et al., 2008). We found expression of D1 and A2a receptor mRNAs to be consistently highly segregated across striatal subregions, and consistently less than the lower estimates for BAC transgenic mice (4%, Wei et al., 2018). Importantly, *iCre* specificity for the off-target pathway was extremely low across striatal subregions in both lines. It is worth noting however that using the native *Drd1a* promoter may not entirely restrict Cre expression to dMSNs - for example, a subset of fast-spiking interneurons has been found to express D1 receptors (Bracci, Centonze, Bernardi, & Calabresi, 2002).

Although the present characterization has focused on the striatum, A2a receptors are also found in the cortex, globus pallidus, hippocampus, thalamus, cerebellum (Rosin, Robeva, Woodard, Guyenet, & Linden, 1998), and throughout the cardiovascular system. Similarly, D1 receptor mRNA has been localized in prefrontal cortex, hippocampus, thalamus and hypothalamus (Fremeau et al., 1991). Thus, our new rats will support investigations of adenosinergic and dopaminergic signaling in attention, motor control, memory and mood across multiple brain regions. In coordination with a rapidly expanding set of optical and genetic tools, these rats offer the ability to clarify fundamental questions about brain circuitry, with implications for making progress on targeted therapeutics for a range of neurological and psychiatric disorders.

Author contributions

TLS and JDB designed the *A2a-Cre and D1-Cre* constructs. EDH prepared the genome editing reagents. WEF performed rat zygote microinjections. MGZ performed genotyping and identification of C3 mutations. JYY and JRP analyzed the FISH data. RCD performed and analyzed the behavioral experiments, which were supervised by CF. JDB conceived and supervised the project, and edited the manuscript. JRP performed the FISH and viral tracing experiments, and wrote the manuscript with input from all authors.

Acknowledgements

Support for this work was provided by the National Institute on Drug Abuse, the National Institute on Neurological Disorders and Stroke, the National Institute of Mental Health, the CHDI Foundation, The University of Michigan, and the University of California, San Francisco. C.R.F. was supported by NIDDK R01-DK106188. R.C.D. was supported by NIDA T32-DA007281 and NIDDK 1F31-DK111194-01. Support for the Transgenic Animal Model Core of the University of Michigan's Biomedical Research Core Facilities was provided by The University of Michigan Cancer Center, NIH grant number CA46592, The University of Michigan Gut Peptide Research Center, NIH grant number DK34933, and The University of Michigan George M. O'Brien Renal Core Center, NIH grant number P30DK08194.

MATERIALS AND METHODS

All animals were housed in an AAALAC accredited facility in accordance with the National Research Council's guide for the care and use of laboratory animals. All procedures were approved by the University of Michigan's and the University of California San Francisco's Institutional Animal Care & Use Committee.

CRISPR/Cas9 Reagents

CRISPR/Cas9 technology (Cong et al., 2013; Mali, Yang, et al., 2013) was used to generate genetically modified rat strains. Two single guide RNA (sgRNA) targets and protospacer adjacent motifs (PAM) were identified downstream of the rat Adora2a termination codon with the algorithm described by Hsu et al., 2013. The sgRNA targets were cloned into plasmid pX330 (Addgene.org plasmid #42230, a kind gift of Feng Zhang) as described (Ran et al., 2013). The guide targets were C30G1: 5' CTA AGG GAA GAG AAA CCC AA 3' PAM: TGG and C30G2: 5' GGC TGG ACC AAT CTC ACT AA 3' PAM: GGG. Circular pX330 plasmid DNA containing each sgRNA was purified with an endotoxin-free kit (Qiagen, Germantown, Maryland). pX330 plasmids were co-electroporated into rat embryonic fibroblasts with a PGKpuro plasmid (McBurney, Fournier, Jardine, & Sutherland, 1994). Genomic DNA was prepared from the cells after transient selection with puromycin (2 μg/ml). Genomic DNA was extracted from the selected cells. A 324 bp DNA fragment spanning the expected Cas9 cut sites was PCR amplified with forward primer 5' GGG ATG TGG AGC TTC CTA CC 3' and reverse primer 5' GCA GCC CTG ACC TAA CAC AG 3' (Fig. 1). DNA sequencing of the amplicons showed that cells treated with C30G1 contained overlapping chromatogram peaks, indicative of multiple templates that differ because of non-homologous endjoning repair of CRISR/Cas9 induced chromosome breaks that results in the presence of small deletions/insertions (indels). Analysis of genomic DNA prepared from cells treated with C30G1 showed the presence of chromosome breaks while C30G2 treatment did not induce chromosome breaks. sgRNA C30G1 was chosen for rat zygote microinjection. A DNA donor was synthesized (BioBasic.com) to introduce the following elements between amino acid codon 410 and the termination codon: a glycine-serine-serine linker with porcine teschovirus-1 self cleaving peptide 2A (P2A, J. H. Kim et al., 2011) followed by iCre recombinase (Shimshek et al., 2002) followed by the influenza hemagglutinin protein tag YPYDVPDYA (Kolodziej & Young, 1991) and a termination codon with the bovine growth hormone polyadenylation sequence (Goodwin & Rottman, 1992). To mediate homologous recombination with the chromosome a 5' arm of homology (1804 bp of genomic DNA 5' to codon 410) and a 3' arm of homology (1424 bp of genomic DNA downstream of the termination codon) were used. The 20 bp sequence of C30G1 was

omitted from the 3' arm of homology to prevent CRISPR/Cas9 cleavage of the chromosome after correct insertion of the DNA donor.

A similar approach was used for D1. Two sgRNA were identified downstream of the D1 termination codon - C31G1: 5' TTC CTT AAC AGC AAG CCC AA 3' PAM: GGG and C31G2: 5' CTG AGG CCA CGA GTT CCC TT 3' PAM: GGG. A 293 bp DNA fragment spanning the expected Cas9 cut sites was PCR amplified with forward primer 5' TGG AAT AGC TAA GCC ACT GGA 3' and reverse primer 5' CTC CCA AAC TGA TTT CAG AGC 3'. Both sgRNAs were found to be active after transfection in rat fibroblasts by T7 endonuclease 1 (T7E1) assays. Amplicons were subjected to T7E1 digestion essentially as described (Sakurai, Watanabe, Kamiyoshi, Sato, & Shindo, 2014). Briefly, DNA amplicons were melted and re-annealed, then subjected to T7EI digestion. The digested DNA fragments were separated by agarose gel electrophoresis. Gels were stained with Sybr Gold (Invitrogen S11494) to detect indels in the amplicon. The presence of indels produced by non-homologous endjoining repair of Cas9-induced double strand breaks resulted in the presence of lower molecular weight DNA fragments in presences of T7E1 for both C31G1 and C31G2 sgRNA targets, indicating that both sgRNA were effective at producing chromosome breaks. sgRNA C31G1 was chosen for rat zygote microinjection. A DNA donor was synthesized (BioBasic.com) to introduce the following elements between D1 amino acid codon 446 and the termination codon: a glycine-serine-serine linker with P2A followed by *iCre* recombinase followed by the V5 peptide tag GKPIPNPLLGLDST (Yang et al., 2013) and a termination codon with the bovine growth hormone polyadenylation sequence. To mediate homologous recombination with the chromosome a 5' arm of homology (1805 bp of genomic DNA 5' of codon 446) and a 3' arm of homology (1801 bp of genomic DNA downstream of the termination codon) were used. The 20 bp sequence of C31G1 was omitted from the 3' arm of homology to prevent CRISPR/Cas9 cleavage of the chromosome after correct insertion of the DNA donor.

Rat Zygote Microinjection

Rat zygote microinjection was carried out as described (Filipiak & Saunders, 2006). sgRNA molecules from a PCR amplified template for microinjection were obtained by in vitro transcription (MAXIscript T7 Transcription Kit followed by purification with a MEGAclear Transcription Clean-Up Kit - Thermo Fisher Scientific). The template was produced from overlapping long primers (IDTDNA.com) that included one gene specific sgRNA target and T7 promoter sequence that were annealed to a long primer containing the sgRNA scaffold sequence as described (Lin, Staahl, Alla, & Doudna, 2014). Cas9 mRNA was obtained from Sigma-Aldrich (catalog no. CAS9MRNA). Circular DNA donor plasmids were purified with an endotoxin free kit (Qiagen, Germantown, Maryland).

A2a-Cre knockin rats were produced by the microinjection of a solution containing 5 ng/μl Cas9 mRNA, 2.5 ng/μl C30G1 sgRNA, and 10 ng/μl of circular donor plasmid. *D1-Cre* knockin rats were produced by the microinjection of a solution containing 5 ng/μl Cas9 mRNA, 2.5 ng/μl C31G1 sgRNA, and 10 ng/μl of circular donor plasmid. Prior to rat zygote microinjection fertilized mouse eggs were microinjected with the nucleic acid mixtures to ensure that the plasmid DNA mixtures did not cause zygote death or block development to the blastocyst stage. Rat zygotes for microinjection were obtained by mating superovulated Long Evans female rats with Long Evans male rats from an in-house breeding colony. 353 rat zygotes were microinjected with Adora2a-iCre reagents, 289 survived and were transferred to pseudopregnant SD female rats (Strain Code 400, Charles River Laboratories). Genomic DNA was from obtained from 60 rat pups born after transfer. 401 rat zygotes were microinjected with D1-Cre reagents, 347 survived and were transferred to pseudopregnant SD female rats. Genomic DNA was obtained from 95 pups born after transfer. Genomic DNA was purified from tail tip biopsies (Qiagen DNeasy kit) and used to screen potential founders for correct insertion of *iCre*.

G0 Founder Screening Primers

iCre internal primers for both lines

iCre FWD 5' AAT GTG AAC ATT GTG ATG AAC TAC A 3'
iCre REV 5' CAG AAT AGA ATG ACA CCT ACT CAG ACA 3'

Insertion-spanning primers for A2a-Cre

5' Junction FWD: 5' AGG CAA CTT TCT AGT TGA CAA ATC AAG 3'
5' Junction REV: 5' CAG CAG GCT GAA GTT AGT AGC TC 3'

3' Junction FWD: 5' CAT TGT CTG AGT AGG TGT CAT TCT ATT CT 3'
3' Junction REV: 5' GAA TCA CAG CCC AAG AGA TAC TAC ACT 3'

Insertion-spanning primers for D1-Cre

5' Junction FWD: 5' AAA AGT GAC TAG AAT TGA CCT GGA AGA G 3'
5' Junction REV: 5' AGC AGG TTG GAG ACT TTC CTC TTC TTC TT 3'

3' Junction FWD: 5' CAT TGT CTG AGT AGG TGT CAT TCT ATT CT 3'
3' Junction REV: 5' GGA AAA GGA AAG AGA AGC AGA ATA AT 3'

Colony management and genotyping

The lines were maintained by backcrossing each generation with wildtype rats (Charles River) for a minimum of 5 generations. Offspring were genotyped using real-time PCR (Transnetyx).

A2a-Cre insertion-spanning primers:

FWD: 5' CGT CTC CAG CCT GCT TCA G 3'
REV: 5' TCC TCA TGG TCT TCA GAG TTT GC 3'
Reporter 1: 5' CCG GAA GCG GAG CTA C 3'

D1-Cre insertion-spanning primers:

FWD: 5' GTG AGG CTG CTC GAG GAT 3'
REV: 5' CTG GCA ACT AGA AGG CAC AGT 3'
Reporter 1: 5' CCT GGA CAG CAC CTG AC 3'

mRNA fluorescence *in situ* hybridization

Brains were removed from animals after deep isoflurane anesthesia and submerged in Optimal Cutting Temperature cutting medium (Tissue-Tek) over powdered dry ice. Frozen brains were stored in an airtight container at -80C (~overnight- 2 weeks). Brains were sectioned on a cryostat at 20 μm, mounted on glass slides and stored overnight in an airtight container at -80C. Sections were fixed in 4% PFA at 4C for 15 minutes and dehydrated through 50%, 75%, 100% and fresh 100% EtOH at RT for 5 minutes each. Slides were dried completely for 5 minutes. A hydrophobic barrier (Advanced Cell Diagnostics) was drawn around each section and allowed to dry ~1 minute. Slides were rinsed twice in 1xPBS (~1-3 minutes) and incubated with Protease IV reagent (Advanced Cell Diagnostics) for 30 minutes at RT. Fluorescent probes (RNAScope, Advanced Cell Diagnostics, *iCre* Cat. 312281, *D1* Cat. 317031-C2 and *Adora2a* Cat. 450471-C3) were added to each slide (2 hours, 40C) followed by manufacturer-specified washing and amplification. DAPI was added to the slides before being cover slipped (Prolong Gold, Thermo Fisher Scientific).

Virus injection surgery

Rats (n=1 from each line) were anesthetized under isofluorane and fixed in a stereotax. They were next microinjected with 0.5 μL of CAG-Flex-TdTomato virus in dorsal striatum at three locations along a dorsal-ventral trajectory (AP: +1.5, ML: +2.2, DV: -

3.0, -4.0, -5.0 from brain surface). Rats were allowed to recover in their home cage and euthanized 4 weeks after surgery.

Imaging

Images for fluorescent in situ hybridization and viral tracing were taken with a Nikon spinning disc confocal microscope with a 40X objective (Plan Apo Lambda NA 0.95). Images were acquired at 2048x2048 pixels at 16bit depth and stitched in FIJI imaging software for viral tracing.

Quantification of mRNA fluorescent *in situ* hybridization

We used the MIPAR image analysis software (www.mipar.us) to segment cell boundaries and fluorescent puncta using separate processing pipelines. The DAPI channel of each image was used to define nucleus boundaries, which were segmented as follows. The image was first histogram equalized to compensate for uneven illumination (512x512 pixel tiles) and convolved with a pixel-wise adaptive low-pass Wiener filter (5x5 pixel neighborhood size) to reduce noise. The image was then contrast adjusted to saturate the top and bottom 1% of intensities. Bright pixels were segmented as objects using an adaptive threshold, defined as the pixel intensity greater than 110% of mean in the surrounding 30-pixel window. Image erosion followed by dilation was used to reduce noise (5-pixel connectivity threshold, 10 iterations). The Watershed algorithm was applied to improve object separation. Objects larger than 5000 pixels (i.e. clustered nuclei) were identified and reprocessed to improve separation within the cluster. Since mRNA fluorescent puncta can be located in the endoplasmic reticulum surrounding the nuclei, we dilated the boundaries of each segmented nuclei by 5 pixels to include these regions.

For segmenting fluorescent puncta, we used the following steps. To reduce noise and improve contrast, images were filtered using a Top-hat filter (9-15-pixel radius), Wiener

filter (15x15 pixel neighborhood size) followed by contrast adjustment to saturate the top and bottom 1% of intensities. Bright regions were segmented using the extended-maxima transform (8-connected neighborhood, 5 H-maxima). A Watershed algorithm followed by erosion was used to improve object separation. Objects with less than 5 pixels were rejected as noise. The location of each puncta is defined as the centroid of the segmented object. This was done individually for each of the three fluorescent probe image channels.

For each fluorescent probe image channel, we counted the number of segmented puncta objects lying within a nucleus' boundary. Since there can be puncta located outside of nuclei from non-specific probe hybridization, we needed to estimate the "baseline" number of puncta expected per nucleus by chance while taking the background into account. To determine the baseline, we counted all puncta lying outside of cell nuclei and divided this value by the number of pixels in the image. This is the expected puncta count expressed as puncta per pixel. To calculate a distribution for the expected number of puncta per nucleus, we multiplied the expected puncta per pixel by the number of pixels for each DAPI-labelled nucleus in the image. We assumed that the puncta count per nucleus follows a Poisson distribution with a mean corresponding to the expected puncta count per nucleus, and used the puncta count corresponding to the 99.9^{th} percentile of the distribution as the background threshold. Cells that exceeded this count were categorized as positive for that mRNA probe. This categorization was used to calculate the consistency and specificity of *iCre* in each line.

Consistency was calculated as the percentage of *A2a+ or D1+* nuclei that also had above-threshold counts of *iCre* puncta. Specificity was calculated as the percentage of *iCre+* nuclei that also had above-threshold counts of *A2a or D1* puncta.

Behavioral Testing

Subjects: Heterozygous D1-Cre and A2a-Cre rats were bred to wild type Long Evans rats obtained from Harlan. *Cre+* and *Cre-* littermates (male and female) were used. Rats

were maintained on a reverse light-dark schedule (12/12) and all testing was conducted during the dark phase of the cycle.

Apparatus: For locomotor testing, testing was conducted in rectangular plastic chambers (25.4 cm X 48.26cm X 20.32 cm) sitting within a frame outfitted with photocell arrays around the base perimeter. Beam breaks were measured using CrossBreak data collection software (Synaptech; University of Michigan). For instrumental and Pavlovian conditioning, standard operant chambers (Med-Associates) housed within sound- and light-attenuating cabinets were used. Each chamber was outfitted with a white noise generator, tone generator, and pellet dispenser that delivered pellets into a recessed food cup. The food cup was flanked by two retractable levers. Every cabinet was equipped with a Jamicon 24V ventilation fan and a strip of red LED lights affixed to the inner wall of the cabinet was used for background illumination. Prior to the start of training, food was removed from the home cages and rats were slowly brought down to 85-90% of their free-feeding body weight across 3 days. Rats were weighed daily and food rations were titrated to maintain this reduced body weight for the duration of training.

Assessment of Cocaine Induced Locomotor Activity: Locomotor activity was assessed in a subset of the rats trained above (*Cre-,* n= 7; *D1 Cre*+, n= 7; *Adora2a Cre*+, n= 7). For these tests food restriction was lifted and rats were fed ad lib for at least 5 days prior to testing. Rats were habituated to the testing chamber and IP injections prior for 2 sessions. Each session lasted 120 minutes. After the first 30 minutes rats were given an IP injection of saline and immediately returned to the testing chambers. After 45 minutes, a second IP injection of saline was administered and the rats were placed back into the testing chambers for an additional 45 minutes. After which rats were returned to their homecages. Photocell beam breaks were recorded throughout this 120-minute session and collected in 5 minute bins to provide a readout of locomotor activity within the chambers.

After this habituation phase rats underwent a test to assess locomotor response to acute cocaine administration. As in the habituation sessions, rats were placed into the

locomotor chambers and after 30 minutes were given an IP injection of saline. Forty-five minutes later, rats were given a 15mg/kg IP injection of cocaine and returned to the locomotor chambers for an additional 60 minutes of monitoring. Locomotor activity was recorded throughout this 135-minute test session.

Instrumental Training: To evaluate instrumental learning, rats were trained on an instrumental discrimination task using levers (*D1-Cre*-, n= 9 [3m, 6f]; *D1-Cre*+, n= 16 [7m, 9f]; *A2a-Cre*-, n= 8 [6m, 2f]; *A2a-Cre*+, n= 16 [10m, 6f]). Prior to this instrumental training, rats were given two 20-minute sessions of food cup training on separate days. In this session 20 pellets (45 mg, Bioserv Rodent Purified Dustless Precision Pellets; Product # F0021) were delivered on a variable-interval schedule of 60 sec (VI60"). During instrumental training, two levers were inserted into the chambers at the start of the session and remained present for the duration of each session; presses on the 'active' lever generated delivery of a single pellet (fixed ratio 1; FR1) whereas presses on the other 'inactive' lever did not generate any consequences. Active and inactive lever positions were counterbalanced across rats. Rats were trained to an acquisition criterion of 50 pellets consecutively within a maximum 40-minute session duration. The session terminated if rats reached this criterion or if 40 minutes had lapsed without this criterion being reached. When necessary, rats were given multiple training sessions until reaching the acquisition criterion. The total time (across sessions) to acquire the task, the total number of active and inactive lever responses, and total number of pellets earned were measured.

Pavlovian Training: Training procedures were the similar to those previously reported (Derman & Ferrario, 2018). In this Pavlovian discrimination task, rats were trained with two auditory conditioned stimuli (CS; tone and white noise). The CS+ was paired with pellet delivery and a CS- was presented an equal number of times, but never paired with pellets. Rats received 12, 60-minute training sessions in which each CS was randomly presented 4 times/session (CS+/CS- assignments counterbalanced). Each CS presentation lasted 2 minutes and on CS+ trials 4 pellets were delivered on a VI30 schedule (range: 15-45 sec). Trials were separated by a variable 5 min inter-trial-interval (ITI; range: 3-7 minutes). Food cup entries during the CS+, CS-, and ITI were recorded

in 10 sec bins throughout each session. Food cup entries during the first 10 seconds of CS presentations were used to evaluate conditioned anticipatory responding as the earliest possible pellet delivery could occur 15 seconds following CS+ onset.

FIGURE LEGENDS

Figure 1. Details of insertion design and founder line screening.
(A) Schematic of insertion cassettes into *Adora2a* (above) and *Drd1a* (below) genes. (Abbreviations: P2A, porcine teschovirus-1 self cleaving peptide; NLS, nuclear localization sequence; HA, influenza hemagglutinin protein tag YPYDVPDYA; V5, peptide tag GKPIPNPLLGLDST; bGH, bovine growth hormone polyadenylation sequence). (B) PCR primer loci (above) and corresponding gels (below) for G0 screening of the A2a-Cre line. See Methods for full primer sequences for screening both lines.

Figure 2. Confirmation and quantification of *iCre* production in D1+ and A2a+ MSNs.
(A) Example 40X images of FISH labelling used for quantification, taken from dorsal striatum (scale bars = 50 μm). (B) Closeups from the 40X images in panel A aligned with their corresponding automated software output. Gray regions indicate DAPI boundaries and colored dots indicate puncta within DAPI boundaries, using the same color scheme from panel A. Gray dots indicate the locations of puncta detected outside of DAPI boundaries. (C) Scatterplots of raw puncta counts for each cell show selective *iCre* mRNA co-localization with the target receptor mRNA. Black, crimson and red threshold lines indicate the 50th, 95th and 99.9th confidence limits for the Poisson distribution of baseline puncta expected by chance, respectively. Subpanels are grouped into rows by striatal region and into columns by genotype. Atlas images depict the locations of confocal images used for mRNA quantification. (D) Functional *iCre* expression is confined to appropriate BG pathways: (left) CAG-Flex-TdTomato injected into DS of the D1-Cre line expresses in terminals in SNr/GPi but not GPe. (right) CAG-

Flex-TdTomato injected into DS of the A2a-Cre line expresses in terminals in GPe but not SNr/GPi.

Figure 3. Basal and cocaine induced locomotor activity is similar between mutant lines and *iCre*- littermate controls.

(A) The average number of crossover events, or beam breaks of the photocells lining the perimeter of the operant chamber, decreases over time and does not differ between genotypes during habituation training. (B) The average number of crossovers increases in response to saline but not cocaine injections, with no differences between genotypes. (C) The average total number of crossovers is greater in the 45 minutes following cocaine injections vs the 45 minutes following saline injections, with no differences between genotypes. All data represented as mean ± SEM.

Figure 4. Instrumental and Pavlovian discrimination learning is similar between mutant lines and *Cre*- littermate controls.

(A) The average total presses does not differ between groups and all groups press the active lever more than the inactive lever; * = $p < 0.05$ active vs. inactive responses. (B) The total time to reach the FR1 acquisition criterion does not differ between groups. (C) The average rate of food cup entries during the first 10 seconds of CS+ presentations increases across 2-session training blocks and does not differ between groups. (C) The average rate of food cup entries during the first 10 seconds of CS- presentations does not change across training blocks and does not differ between groups. (C) The average latency to approach the food cup following CS+ onset rapidly deceases across training blocks and does not differ between groups. (D) The average latency to approach the food cup following CS- increases across training blocks and does not differ between groups. Dotted line denotes the 15 seconds to indicate scale difference between panels C and D. All data represented as mean ± SEM.

References

Alcantara, A. A., Chen, V., Herring, B. E., Mendenhall, J. M., & Berlanga, M. L. (2003). Localization of dopamine D2 receptors on cholinergic interneurons of the dorsal striatum and nucleus accumbens of the rat. *Brain Research*, *986*(1–2), 22–29. https://doi.org/10.1016/S0006-8993(03)03165-2

Barbera, G., Liang, B., Zhang, L., Gerfen, C. R., Culurciello, E., Chen, R., … Lin, D.-T. (2016). Spatially Compact Neural Clusters in the Dorsal Striatum Encode Locomotion Relevant Information. *Neuron*, *92*(1), 202–213. https://doi.org/10.1016/J.NEURON.2016.08.037

Berke, J. D. (2018). What does dopamine mean? *Nature Neuroscience*, *21*(6), 787–793. https://doi.org/10.1038/s41593-018-0152-y

Berke, J. D., Paletzki, R. F., Aronson, G. J., Hyman, S. E., & Gerfen, C. R. (1998). A complex program of striatal gene expression induced by dopaminergic stimulation. *The Journal of Neuroscience : The Official Journal of the Society for Neuroscience*, *18*(14), 5301–10. https://doi.org/10.1523/JNEUROSCI.18-14-05301.1998

Bertran-Gonzalez, J., Bosch, C., Maroteaux, M., Matamales, M., Hervé, D., Valjent, E., & Girault, J.-A. (2008). Opposing patterns of signaling activation in dopamine D1 and D2 receptor-expressing striatal neurons in response to cocaine and haloperidol. *The Journal of Neuroscience : The Official Journal of the Society for Neuroscience*, *28*(22), 5671–5685. https://doi.org/10.1523/JNEUROSCI.1039-08.2008

Bracci, E., Centonze, D., Bernardi, G., & Calabresi, P. (2002). Dopamine Excites Fast-Spiking Interneurons in the Striatum. *Journal of Neurophysiology*, *87*(4), 2190–2194. https://doi.org/10.1152/jn.00754.2001

Collins, A. G. E., & Frank, M. J. (2014). Opponent actor learning (OpAL): modeling interactive effects of striatal dopamine on reinforcement learning and choice incentive. *Psychological Review*, *121*(3), 337–66. https://doi.org/10.1037/a0037015

Cong, L., Ran, F. A., Cox, D., Lin, S., Barretto, R., Habib, N., … Zhang, F. (2013). Multiplex genome engineering using CRISPR/Cas systems. *Science (New York, N.Y.)*, *339*(6121), 819–23. https://doi.org/10.1126/science.1231143

Cui, G., Jun, S. B., Jin, X., Pham, M. D., Vogel, S. S., Lovinger, D. M., & Costa, R. M. (2013). Concurrent activation of striatal direct and indirect pathways during action initiation. *Nature*, *494*(7436), 238–242. https://doi.org/10.1038/nature11846

Day, M., Wang, Z., Ding, J., An, X., Ingham, C. A., Shering, A. F., … Surmeier, D. J. (2006). Selective elimination of glutamatergic synapses on striatopallidal neurons in Parkinson disease models. *Nature Neuroscience*, *9*(2), 251–259. https://doi.org/10.1038/nn1632

Derman, R. C., & Ferrario, C. R. (2018). Enhanced incentive motivation in obesity-prone rats is mediated by NAc core CP-AMPARs. *Neuropharmacology*, *131*, 326–336. https://doi.org/10.1016/J.NEUROPHARM.2017.12.039

Filipiak, W. E., & Saunders, T. L. (2006). Advances in transgenic rat production. *Transgenic Research*, *15*(6), 673–686. https://doi.org/10.1007/s11248-006-9002-x

Fremeau, R. T., Duncan, G. E., Fornaretto, M. G., Dearry, A., Gingrich, J. A., Breese, G. R., & Caron, M. G. (1991). Localization of D1 dopamine receptor mRNA in brain supports a role in cognitive, affective, and neuroendocrine aspects of dopaminergic neurotransmission. *Proceedings of the National Academy of Sciences of the United States of America*, *88*(9), 3772–6. https://doi.org/10.1073/PNAS.88.9.3772

Gerfen, C. R., & Surmeier, D. J. (2011). Modulation of Striatal Projection Systems by Dopamine. *Annual Review of Neuroscience*, *34*(1), 441–466. https://doi.org/10.1146/annurev-neuro-061010-113641

Goodwin, E. C., & Rottman, F. M. (1992). The 3'-flanking sequence of the bovine growth hormone gene contains novel elements required for efficient and accurate polyadenylation. *Journal of Biological Chemistry*, *267*(23), 16330–16334.

Hamid, A. A., Pettibone, J. R., Mabrouk, O. S., Hetrick, V. L., Schmidt, R., Vander Weele, C. M., … Berke, J. D. (2015). Mesolimbic dopamine signals the value of work. *Nature Neuroscience*, *19*(1), 117–126. https://doi.org/10.1038/nn.4173

Heintz, N. (2004). Gene Expression Nervous System Atlas (GENSAT). *Nature Neuroscience*, *7*(5), 483–483. https://doi.org/10.1038/nn0504-483

Hsu, P. D., Scott, D. A., Weinstein, J. A., Ran, F. A., Konermann, S., Agarwala, V., … Zhang, F. (2013). DNA targeting specificity of RNA-guided Cas9 nucleases. *Nature Biotechnology*, *31*(9), 827–832. https://doi.org/10.1038/nbt.2647

Jung, C. J., Ménoret, S., Brusselle, L., Tesson, L., Usal, C., Chenouard, V., … Anegon, I. (2016). Comparative Analysis of piggyBac, CRISPR/Cas9 and TALEN Mediated BAC Transgenesis in the Zygote for the Generation of Humanized SIRPA Rats. *Scientific Reports*, *6*(1), 31455. https://doi.org/10.1038/srep31455

Kim, J. H., Lee, S.-R., Li, L.-H., Park, H.-J., Park, J.-H., Lee, K. Y., … Choi, S.-Y. (2011). High Cleavage Efficiency of a 2A Peptide Derived from Porcine Teschovirus-1 in Human Cell Lines, Zebrafish and Mice. *PLoS ONE*, *6*(4), e18556. https://doi.org/10.1371/journal.pone.0018556

Kim, Y.-C., Han, S.-W., Alberico, S. L., Ruggiero, R. N., De Corte, B., Chen, K.-H., & Narayanan, N. S. (2017). Optogenetic Stimulation of Frontal D1 Neurons Compensates for Impaired Temporal Control of Action in Dopamine-Depleted Mice. *Current Biology*, *27*(1), 39–47. https://doi.org/10.1016/J.CUB.2016.11.029

Kolodziej, P. A., & Young, R. A. (1991). Epitope tagging and protein surveillance (pp. 508–519). https://doi.org/10.1016/0076-6879(91)94038-E

Kravitz, A. V., Freeze, B. S., Parker, P. R. L., Kay, K., Thwin, M. T., Deisseroth, K., & Kreitzer, A. C. (2010). Regulation of parkinsonian motor behaviours by optogenetic control of basal ganglia circuitry. *Nature*, *466*(7306), 622–626. https://doi.org/10.1038/nature09159

Kravitz, A. V, Tye, L. D., & Kreitzer, A. C. (2012). Distinct roles for direct and indirect pathway striatal neurons in reinforcement. *Nature Neuroscience*, *15*(6), 816–818. https://doi.org/10.1038/nn.3100

Le Moine, C., & Bloch, B. (1995). D1 and D2 dopamine receptor gene expression in the rat striatum: Sensitive cRNA probes demonstrate prominent segregation of D1 and D2 mRNAS in distinct neuronal populations of the dorsal and ventral striatum. *The Journal of Comparative Neurology*, *355*(3), 418–426. https://doi.org/10.1002/cne.903550308

Lin, S., Staahl, B., Alla, R. K., & Doudna, J. A. (2014). Enhanced homology-directed human genome engineering by controlled timing of CRI SPR / Cas9 delivery. *ELife*, (December). https://doi.org/10.7554/eLife.04766

Mali, P., Esvelt, K. M., & Church, G. M. (2013). Cas9 as a versatile tool for engineering biology. *Nature Methods*, *10*(10), 957–963. https://doi.org/10.1038/nmeth.2649

Mali, P., Yang, L., Esvelt, K. M., Aach, J., Guell, M., DiCarlo, J. E., … Church, G. M.

(2013). RNA-Guide Human Genome Engineering via Cas9. *Science*, *339*(2013), 823–826. https://doi.org/10.1107/S1600536812033132

Matamales, M., Bertran-Gonzalez, J., Salomon, L., Degos, B., Deniau, J.-M., Valjent, E., … Girault, J.-A. (2009). Striatal Medium-Sized Spiny Neurons: Identification by Nuclear Staining and Study of Neuronal Subpopulations in BAC Transgenic Mice. *PLoS ONE*, *4*(3), e4770. https://doi.org/10.1371/journal.pone.0004770

McBurney, M. W., Fournier, S., Jardine, K., & Sutherland, L. (1994). Intragenic regions of the murinePgk-1 locus enhance integration of transfected DNAs into genomes of embryonal carcinoma cells. *Somatic Cell and Molecular Genetics*, *20*(6), 515–528. https://doi.org/10.1007/BF02255842

Ran, F. A., Hsu, P. D., Wright, J., Agarwala, V., Scott, D. A., & Zhang, F. (2013). Genome engineering using the CRISPR-Cas9 system. *Nature Protocols*, *8*(11), 2281–2308. https://doi.org/10.1038/nprot.2013.143

Rosin, D. L., Robeva, A., Woodard, R. L., Guyenet, P. G., & Linden, J. (1998). Immunohistochemical localization of adenosine A2A receptors in the rat central nervous system. *The Journal of Comparative Neurology*, *401*(2), 163–186. https://doi.org/10.1002/(SICI)1096-9861(19981116)401:2<163::AID-CNE2>3.0.CO;2-D

Sakurai, T., Watanabe, S., Kamiyoshi, A., Sato, M., & Shindo, T. (2014). A single blastocyst assay optimized for detecting CRISPR/Cas9 system-induced indel mutations in mice. *BMC Biotechnology*, *14*, 1–11. https://doi.org/10.1186/1472-6750-14-69

Schmidt, R., Leventhal, D. K., Mallet, N., Chen, F., & Berke, J. D. (2013). Canceling actions involves a race between basal ganglia pathways. *Nature Neuroscience*, *16*(8), 1118–24. https://doi.org/10.1038/nn.3456

Shimshek, D. R., Kim, J., Hübner, M. R., Spergel, D. J., Buchholz, F., Casanova, E., … Sprengel, R. (2002). Codon-improved Cre recombinase (iCre) expression in the mouse. *Genesis*, *32*(1), 19–26. https://doi.org/10.1002/gene.10023

Shuen, J. A., Chen, M., Gloss, B., & Calakos, N. (2008). Drd1a-tdTomato BAC Transgenic Mice for Simultaneous Visualization of Medium Spiny Neurons in the Direct and Indirect Pathways of the Basal Ganglia. *Journal of Neuroscience*, *28*(11), 2681–2685. https://doi.org/10.1523/JNEUROSCI.5492-07.2008

Wei, X., Ma, T., Cheng, Y., Huang, C. C. Y., Wang, X., Lu, J., & Wang, J. (2018). Dopamine D1 or D2 receptor-expressing neurons in the central nervous system. *Addiction Biology*, *23*(2), 569–584. https://doi.org/10.1111/adb.12512

Yang, H., Wang, H., Shivalila, C. S., Cheng, A. W., Shi, L., & Jaenisch, R. (2013). One-Step Generation of Mice Carrying Reporter and Conditional Alleles by CRISPR/Cas-Mediated Genome Engineering. *Cell*, *154*(6), 1370–1379. https://doi.org/10.1016/J.CELL.2013.08.022

Figure 1

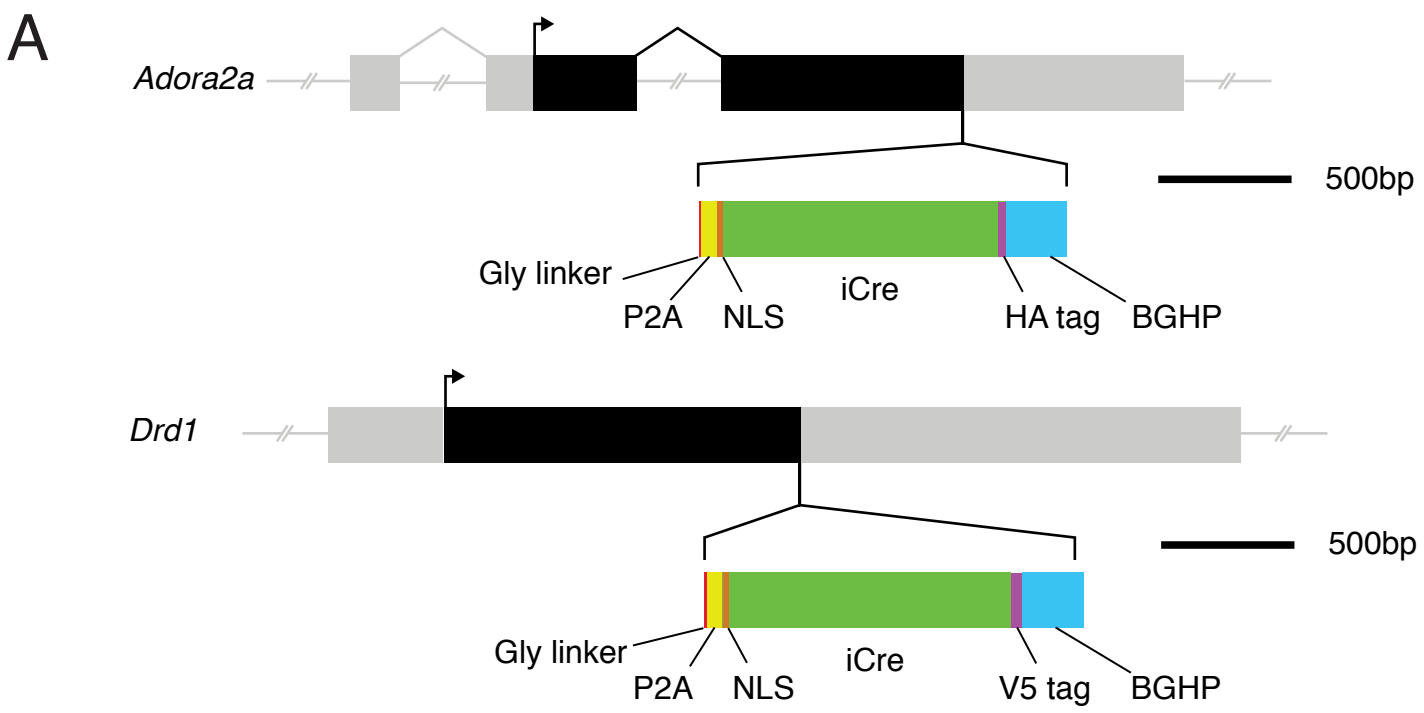

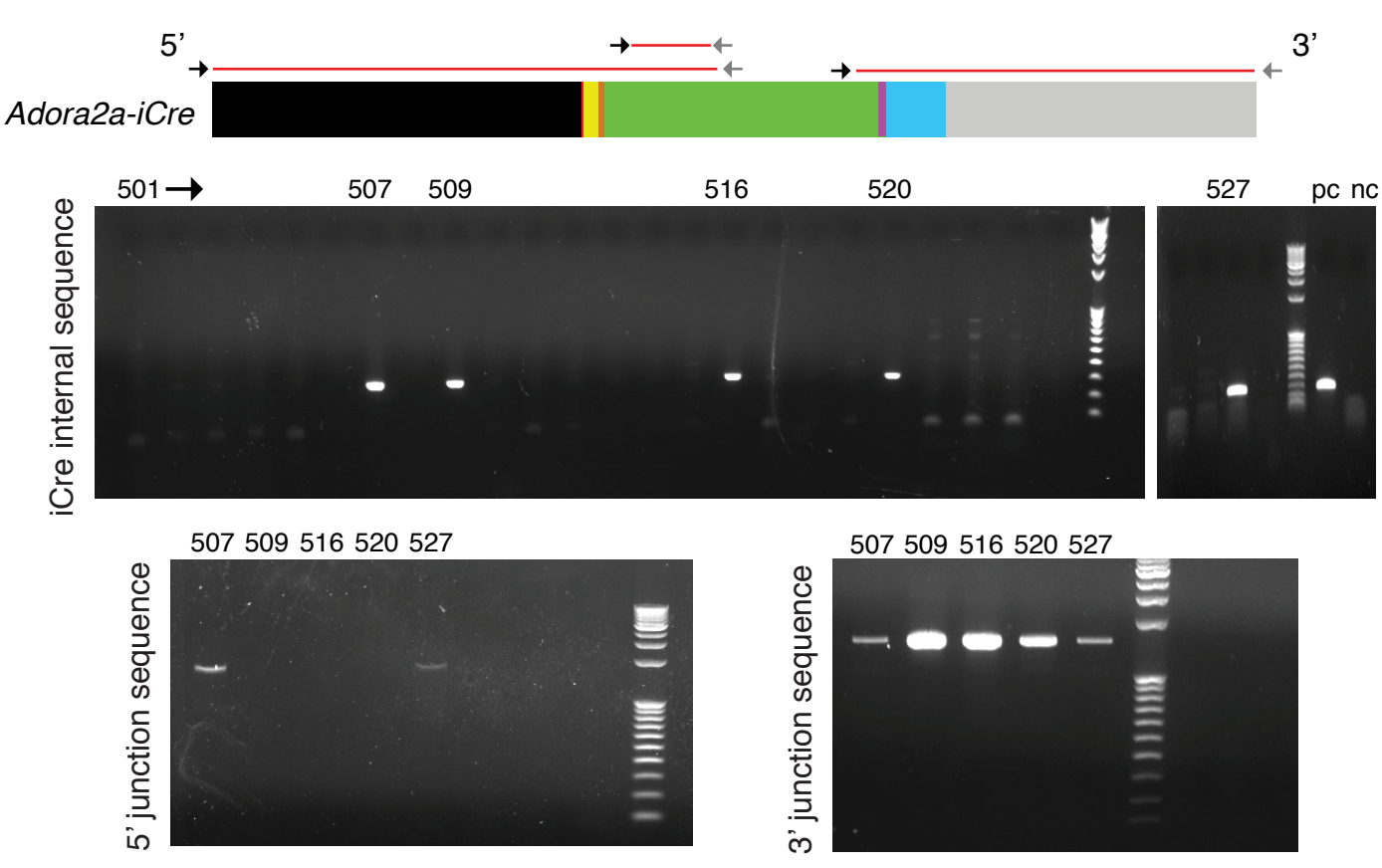

Figure 2

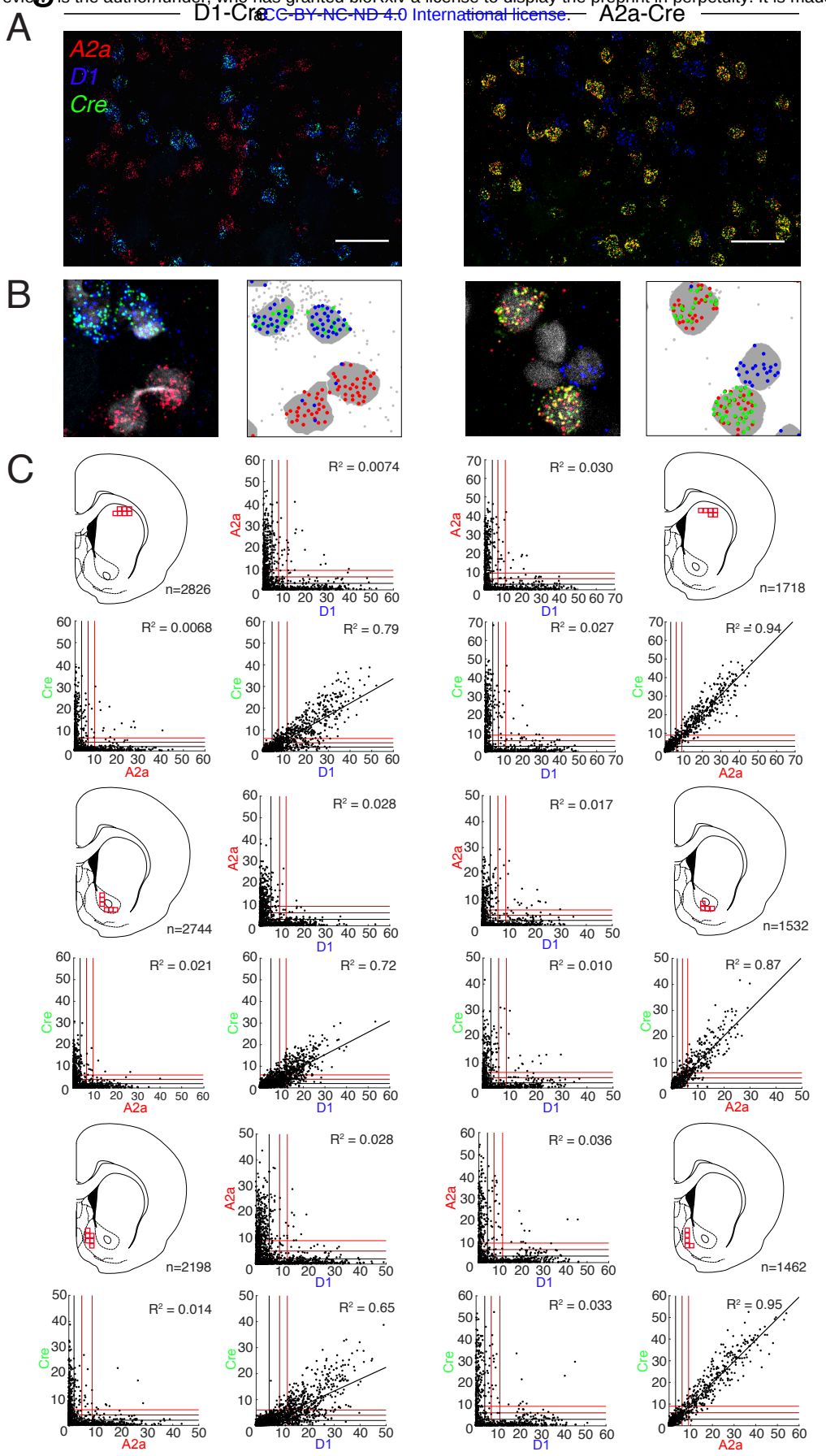

Figure 3

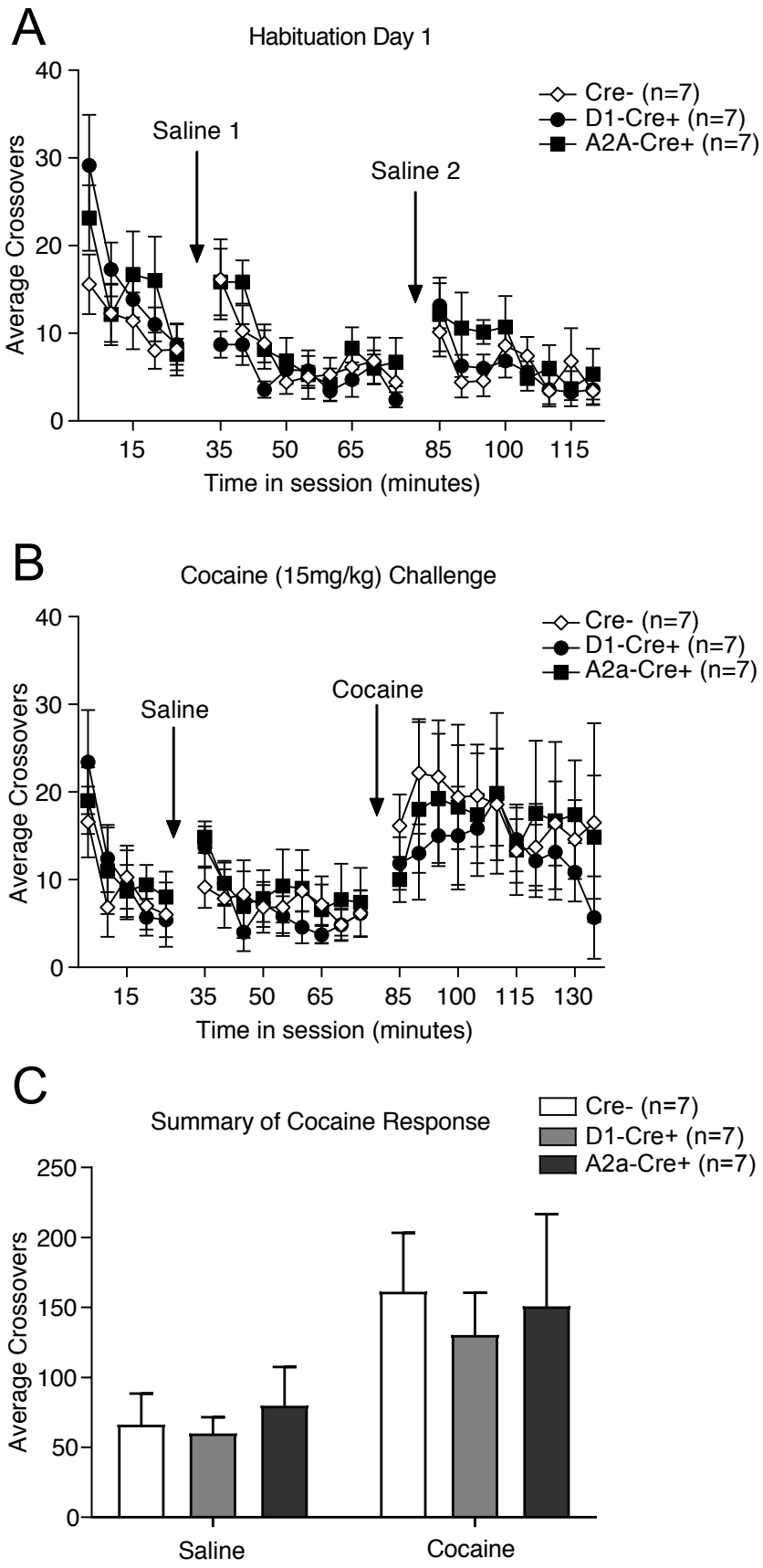

Figure 4